Available online at www.sciencedirect.com
SCIENCE DIRECT®
Ocean Modelling 12 (2006) 268–289
Ocean Modelling
www.elsevier.com/locate/ocemod

Directed drifter launch strategies for Lagrangian data assimilation using hyperbolic trajectories

Anne Molcard [a,b], Andrew C. Poje [c], Tamay M. Özgökmen [a,*]

[a] *RSMAS/MPO, University of Miami, Miami, FL, USA*
[b] *Consiglio Nazionale Delle Rieerche, ISAC, Torino, Italy*
[c] *Department of Mathematics, College of Staten Island, Staten Island, NY, USA*

Received 11 March 2005; received in revised form 10 May 2005; accepted 7 June 2005
Available online 25 July 2005

Abstract

The dependence of the fidelity of a Lagrangian data assimilation scheme on the initial launch locations of the observed drifters is studied in the context of a reduced gravity, primitive equation model of mid-latitude circulations. A directed launch strategy, based on tracking the Lagrangian manifolds emanating from strongly hyperbolic regions in the flow field, is developed. In a series of twin assimilation experiments, the rate of convergence of the data assimilating scheme is shown to be consistently higher in such directed launches compared to those produced from randomly selected initial drifter positions. By directing initial drifter positions along the out-flowing branch of identifiable Lagrangian boundaries, the relative dispersion of the drifters, the overall data coverage and the sampling of high kinetic energy features in the flow are optimized. In general, the performance of the assimilation procedure is shown to depend strongly on the independence of the observed drifter trajectories and the temporal persistence of the corrections provided by the data.

1. Introduction

In the last 20 years, the deployment of surface and subsurface buoys has increased drastically, and the scientific community is now focusing on the development of new techniques to maximize

* Corresponding author.
E-mail address: tozgokmen@rsmas.miami.edu (T.M. Özgökmen).

1463-5003/$ - see front matter
doi:10.1016/j.ocemod.2005.06.004

the use of these data. As shown by Davis (1985, 1991), oceanic observations of quasi-Lagrangian floats provide a useful and direct description of lateral advection and eddy dispersal. Data from surface drifters and subsurface floats have been intensively used to describe the main statistics of the general circulation in most of the world ocean, in terms of mean flow structure, second-order statistics and transport properties (e.g., Owens, 1991; Richardson, 1993; Fratantoni, 2001; Zhang et al., 2001; Bauer et al., 2003; Niiler et al., 2003; Reverdin et al., 2003). Translation, swirl speed and evolution of surface temperature in warm-core rings, which are ubiquitous in the oceans, have also been studied with floats by directing launches inside of the eddies (Hansen and Maul, 1991). Trajectories of freely drifting buoys provide estimates of horizontal divergence and vertical velocity in the mixed layer (Poulain, 1993) and the statistics of near-inertial waves responsible for mixing in the upper thermocline (Poulain et al., 1992). Drifters have proved to be robust autonomous platforms with which to observe ocean circulation and return data from a variety of sensors. They are naturally suitable in practical problems such as oil spill or floating debris tracking and discharge dispersement calculations.

Traditional Eulerian ocean measurement techniques, such as current meter arrays offer data at fixed locations and are limited by small coverage and sparse sampling. Promising emerging new techniques, such as Doppler radar, can provide accurate high-resolution velocity data, but are restricted to the ocean surface and to coastal areas. Lagrangian instruments that provide real-time information via satellite are directly relevant to the now-casting/forecasting problem. These include near-surface drifters and profiling floats (e.g., Davis, 1996, 1998) moving in the subsurface at a certain level and resurfacing every Δt to communicate. In contrast to fixed mooring data, data obtained along float trajectories presumably contain records of turbulent motion at all scales down to several meters with the scale range increasing as a result of the increased sampling rate provided by GPS technology. Floats also offer wide data coverage, both horizontally and vertically, and the availability of significant data sets collected under operational programs (e.g., WOCE, GOOS, CLIVAR, MFSTEP, ACCE, ARGO) implies that Lagrangian data sets have reached a critical mass in most world oceans (e.g., Davis, 1991; Owens, 1991; Lavender et al., 2002; Fratantoni, 2001; Richardson, 2001; Zhang et al., 2001; Bauer et al., 2003; Zhou et al., 2002; Reverdin et al., 2003).

The ocean general circulation models (OGCMs) are providing increasingly realistic Eulerian velocity fields (e.g., Smith et al., 2000; Garraffo et al., 2001; McClean et al., 2002). Given the sampling characteristics and availability of Lagrangian float data, it is desirable to incorporate this information with the goal of improving the forecast accuracy of such models. The main challenge in assimilating Lagrangian position data in OGCMs is the inherently nonlinear relationship between the observed variable, i.e. the position $\mathbf{r}(t)$, and the prognostic model variable to be modified, i.e. the Eulerian velocity field $\mathbf{u}(\mathbf{r}(t), t)$. A number of earlier studies on Lagrangian data assimilation (e.g., Hernandez et al., 1995; Ishikawa et al., 1996) circumvent this problem by assuming that the Lagrangian velocity, computed by finite difference of successive positions $\Delta\mathbf{r}/\Delta t$, can be approximated as an Eulerian velocity and therefore directly assimilated in the OGCM. This approach, denoted "pseudo-Lagrangian", is accurate when the data sampling period Δt is negligible with respect to the Lagrangian time scale T_L, typically $\approx$1–3 days for ocean surface and $\approx$7–15 days for ocean interior (Griffa, 1996; Veneziani et al., 2004). On the other hand, when Δt is a sizable fraction of T_L, as it is typically the case for ocean measurements, the instantaneous Eulerian and computed Lagrangian velocities do not coincide and the method becomes

inaccurate. Another solution to the problem involves the use of an adjoint method (e.g., Kamachi and O'Brien, 1995), which must however be tailored to the specifics of the OGCM and is computationally expensive.

A simple, computationally efficient and highly portable Lagrangian assimilation method has been developed by Molcard et al. (2003) based on the optimal interpolation approach, which takes into account the Lagrangian nature of the observations. The Eulerian velocity field correction is obtained by minimizing the distance between observed trajectories and the synthetic trajectories generated by the model velocity field. This algorithm has been tested successfully in 1.5 layer quasi-geostrophic (Molcard et al., 2003) and primitive-equation models (Özgökmen et al., 2003), and has been also extended for use in multi-layer primitive-equation models (Molcard et al., 2005) using a vertical regression technique similar to that by Oschlies and Willebrand (1996). Other on-going efforts to develop Lagrangian assimilation techniques are summarized in Ide and Ghil (1997a,b), Ide et al. (2002) and Kuznetsov et al. (2003).

Given this Lagrangian assimilation scheme, we focus on a basic question for operational scenarios: Considering the expense of deploying observational drifter arrays, can initial drifter launch locations be determined that lead to more accurate forecasts/nowcasts of the ocean state? Previous studies of Molcard et al. (2003, 2005) and Özgökmen et al. (2003) did not specifically examine the role played by the choice of initial drifter launch locations on the accuracy of the assimilation. Since the number of drifters present in any one area of the ocean at any specific time will necessarily be relatively small, our aim here is to assess the dependence of a given Lagrangian assimilation scheme on the initial conditions of the observations in a data-limited application.

Generally speaking, optimization of assimilation error over drifter launch location is a difficult task. First, Lagrangian trajectories are difficult to predict given the ubiquitous appearance of "Lagrangian chaos" and the resulting sensitivity to initial conditions in even relatively simple Eulerian velocity fields (e.g., Aref, 1984; Samelson, 1991). Second, the strongly nonlinear relationship between the initial launch location and the resulting assimilation product is poorly understood. Finally, the dimensionality of the optimization problem is extremely high given the combinatorics of choosing even a limited number of drifter launch locations from all possible initial conditions.

In this study, we approach the problem by taking advantage of the recent progress in the development of tools based on dynamical systems theory to address issues of Lagrangian motion in geophysical flows. These techniques focus on identifying hyperbolic trajectories in the Lagrangian frame, characterized by the intersection of a stable manifold (along which fluid particles are attracted toward the hyperbolic point) and an unstable manifold (along which fluid particles are repelled away from the hyperbolic point), from a velocity field displaying complex time variability. Haller and Poje (1998) focused on the transient stagnation points and finite-time analogs of stable and unstable manifolds, and extended the lobe analysis to the treatment of finite-time data. This method was then used to analyze fluid particle pathways in an eddy resolving, barotropic ocean model (Poje and Haller, 1999). Finite time geometric techniques have been successful in locating the boundaries of mesoscale coherent features in the Lagrangian frame (e.g., Coulliette and Wiggins, 2000; Miller et al., 2002). In particular, it has been shown that seeding observations in rapidly stretching regions of the flow in the vicinity of identifiable hyperbolic trajectories leads to quantifiable improvements in the overall reconstruction of Eulerian fields from Lagrangian data (Poje et al., 2002) and the sampling of the Eulerian velocity distribution by drifter observations (Toner and Poje, 2004).

While previous studies of directed launch schemes based on Lagrangian structure information examined proxies for assimilation performance, our goal here is to test such launch strategies directly in the context of an existing Lagrangian assimilation scheme in order to determine if quantifiable improvements in the overall performance of the assimilation can be achieved. As a test case, the Miami Isopycnic Coordinate Ocean Model (MICOM) is used in an idealized 1.5-layer, double-gyre configuration at a Reynolds number sufficient to produce an eddy-shedding central jet. Using knowledge of the Lagrangian boundaries in the model, synthetic drifters from a number of initial configurations are used as input for data-assimilating twin experiments and the rate of convergence of the assimilating simulations to the synthetic truth is measured. Examining the proposed launch strategy in a model situation where both the assimilation routine and the Lagrangian analysis have been previously studied allows us to concentrate directly on the question posed: Can knowledge of Lagrangian geometry be used to select drifter initial conditions which accelerate the convergence of the assimilation scheme?

The paper is organized as follows. The numerical model and Lagrangian assimilation scheme are introduced in Section 2 and in Appendix A. The systematic approaches for calculating directed launch templates are outlined in Section 3. The experimental procedure is described in Section 4, and the results are presented in Section 5. Finally, the principal conclusions and future directions are summarized in Section 6.

2. Circulation model and assimilation procedure

The numerical model used in this study is the Miami Isopycnic Coordinate Ocean Model (MICOM), which is a primitive equation, layered model, well documented in the literature (e.g., Bleck et al., 1992; Bleck and Chassignet, 1994). To isolate the dependence of the assimilation on initial drifter launch location, a simple, single active layer (reduced-gravity) version of this model is used (see Appendix A for model equations). The Eulerian flow field is generated using a MICOM configured to produce a wind-driven double-gyre circulation. This flow field has the advantage of being familiar to oceanographers while exhibiting the complex interaction between Sverdrup gyres, western boundary currents, mid-latitude jet and mesoscale eddies. The model parameters are listed in Table 1 and the reader is referred to the description in Özgökmen et al. (2003) for further details.

Table 1
Parameters of MICOM simulations

Zonal basin size	$L_x = 2000$ km
Meridional basin size	$L_y = 2000$ km
Horizontal grid scale	$\Delta x = \Delta y = 20$ km
Coriolis parameters	$f_0 = 9.3 \times 10^{-5}\ \mathrm{s}^{-1}$, $\beta = 2 \times 10^{-11}\ \mathrm{m}^{-1}\ \mathrm{s}^{-1}$
Layer thickness	$h = 1000$ m
Reduced gravity	$g' = 0.02\ \mathrm{m\ s}^{-2}$
Deformation radius	$R_\mathrm{d} = 42$ km
Wind stress amplitude	$\tau_0 = 0.1\ \mathrm{N\ m}^{-1}$
Lateral viscosity	$\upsilon_\mathrm{H} = 400\ \mathrm{m}^2\ \mathrm{s}^{-1}$
Time step	$\delta t = 1200$ s

The Lagrangian data assimilation technique has been developed in the context of a reduced-gravity quasi-geostrophic model by Molcard et al. (2003), then adopted for use in reduced-gravity (Özgökmen et al., 2003) and multi-layer versions of MICOM (Molcard et al., 2005). The main equations are summarized in Appendix A, and the reader is referred to Molcard et al. (2003) for a complete description of the technique.

Throughout, synthetic drifters are considered to be purely Lagrangian fluid particles whose trajectories obey,

$$\begin{aligned} \frac{\mathrm{d}x}{\mathrm{d}t} &= u(x,y,t), \\ \frac{\mathrm{d}y}{\mathrm{d}t} &= v(x,y,t) \end{aligned} \tag{1}$$

subject to initial conditions $(x(t_0), y(t_0)) = (x_0, y_0)$. Numerically, the trajectory equations are solved by interpolating the gridded velocity data from the model onto the particle location using splines, and then time stepping with a second-order Runge–Kutta routine.

3. Lagrangian dynamics and directed launch template

As stated in Section 1, geometric approaches borrowed from dynamical systems theory have been used to delineate the boundaries, in the Lagrangian frame, of mesoscale coherent features in a number of oceanic studies. In short, the goal of this approach is to construct, for a given Eulerian velocity field, the stable and unstable manifolds emanating from hyperbolic particle trajectories. For flows in the plane, these manifolds are one-dimensional objects which are invariant under the flow and thus act as barriers to particle motion. Knowledge of the manifold location provides a global template for the evolution of sets of tracer initial conditions by splitting the initial condition field into regions of distinct particle dynamics. Of particular interest here is the location and orientation of the hyperbolic region at the intersection of the stable and unstable sets. The near exponential stretching in the neighborhood of the hyperbolic trajectory ensures maximal relative particle dispersion for drifter pairs which straddle this point.

The reduced gravity, double-gyre model velocity field considered is very similar to that studied by geometric methods in Poje and Haller (1999). In particular, the eddy field produced by the meandering central jet results in a flow with identifiable, long-lived coherent structures. As shown in Haller and Poje (1998), the existence of finite-time analogs of classical stable and unstable manifolds is predicated on the existence of slowly evolving, and strongly hyperbolic stagnation points in fixed time snap shots of the Eulerian field. In such cases, it can be shown that stable (unstable) manifolds in the full Lagrangian flow remain close to the stable (unstable) eigenvectors of the corresponding saddle point in frozen time slices of the Eulerian velocity field. The reader is referred to Haller and Poje (1998) and Poje and Haller (1999) for details of the procedures and its application to a similar flow field. A brief explanation of the numerical technique used to construct the manifolds is given below.

Fig. 1a shows contours of the dynamic height field in the energetic region of the control simulation at a reference day (day 45). Over the particular 40-day period of interest, three strongly hyperbolic regions were identified in the flow and the corresponding approximations to the stable

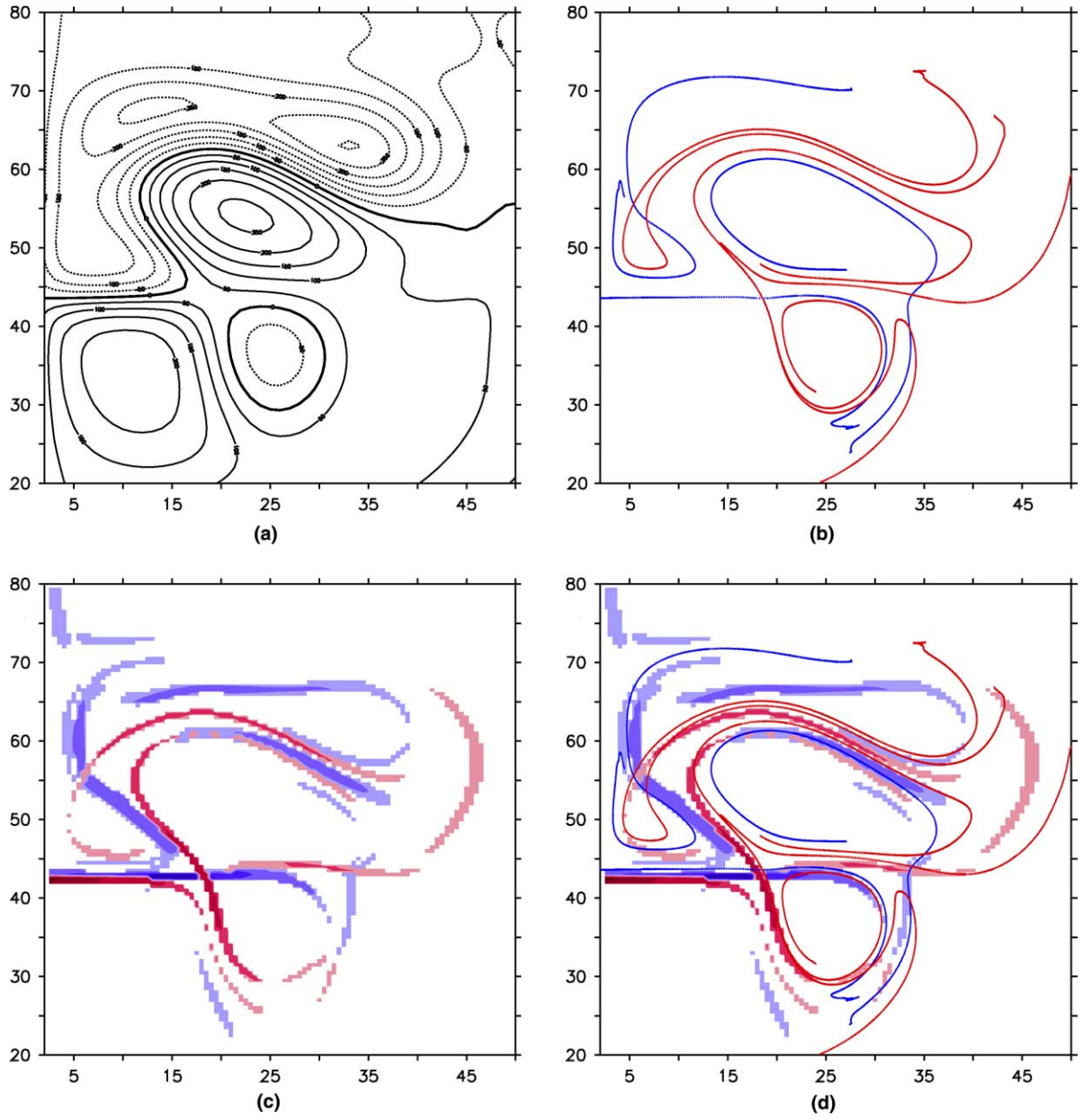

Fig. 1. (a) Layer thickness in the energetic mid-latitude jet region (CI = 50 m) in the Control experiment. (b) In-flowing or stable (blue) and out-flowing or unstable material curves. (c) Contour plot of FSLE (blue: forward in time, red: backward in time). (d) Superposition of the manifolds and FSLE.

and unstable manifolds were constructed using the straddling technique developed in Miller et al. (1997). The resulting geometry is shown in Figs. 1b and 2. Using the location of frozen time saddle points, the unstable manifold is formed by initializing a seed curve along the unstable eigenvector at time t_i and integrating forward in time. As the curve stretches, new trajectories are added in

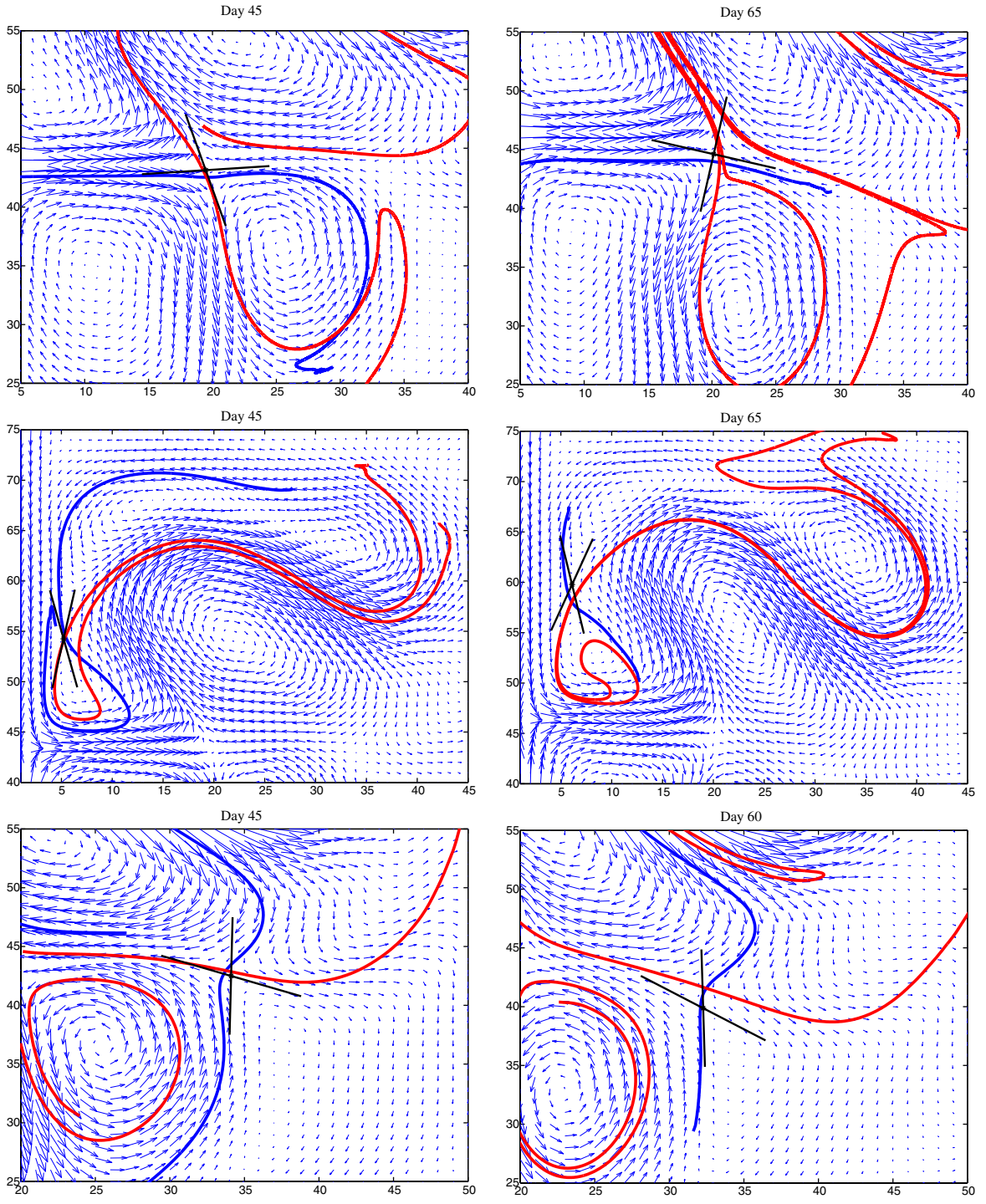

Fig. 2. Model velocity fields showing the location and eigendirections of frozen time Eulerian saddle points (black lines) and the in-flowing (blue lines) and out-flowing (red lines) material curves for the three strongest hyperbolic regions.

order to maintain uniform particle density along the curve. The stable manifold is constructed similarly, initializing along the stable eigenvector at time t_f and integrating backward in time. As shown in Fig. 2, the hyperbolic trajectory, identified by the intersection of the stable and unstable manifolds, remains near the saddle point in frozen-time slices of the Eulerian field for all times during the 30-day period of interest.

The construction of numerical approximations to the stable and unstable sets of individual hyperbolic trajectories requires a fair amount of computational and numerical effort. As an alternative means of identifying high dispersion regions and mixing boundaries upon which to base drifter launch strategies, we also compute the Lagrangian structures produced by the local finite-scale Lyapunov exponent (FSLE) introduced by Aurell et al. (1997) and Artale et al. (1997). The FSLE is a measure of the time required for a pair of particle trajectories to separate a finite distance. Consider an initially uniform distribution of particle positions with initial separation distance δ_i. The FSLE, Λ is given by

$$\Lambda(\mathbf{x}, t, \delta_i, r) = \frac{1}{\tau} \log r, \tag{2}$$

where τ is the time required for a particle pair centered at $\mathbf{x}$ at time t to separate a distance $\delta_f = r\delta_i$. The FSLE converges to the true Lyapunov exponent in the (experimentally unobtainable) double limit of $t \to \infty$ and $\delta_i \to 0$.

Fig. 1c shows the distribution of the FSLE over initial conditions computed by advecting an ensemble of 11,737 particles initialized on a uniform grid with initial separation given by one half the computational grid size, $\delta_i = \Delta\mathbf{x}/2$. These ensembles are advected both forward and backward in time for 90 days. The results are shown for $r = 20$ corresponding to a final separation distance of 100 km. For convenience, both the forward and backward computations are shown on the same plot by assigning negative values to the forward computations.

As shown in Fig. 1d, there is a strong correlation between the geometry of the in-flowing (out-flowing) manifolds and minimum (maximum) values of Λ. Particle pairs initially straddling the in-flowing manifold must eventually encounter near exponential separations in the vicinity of the hyperbolic trajectory. Thus, the time required for the pair to separate $r\delta_i$ will be minimized along the in-flowing (stable) manifolds in the neighborhood of the hyperbolic trajectory. Similarly, for backward time calculations, separation times are minimized along the out-flowing (unstable) manifolds which marks those trajectories which encounter the hyperbolic region in backward time.

In what follows, the exact locations of hyperbolic trajectories, given by the intersection of numerical stable and unstable manifolds, are used to locate drifter initial conditions aligned along the unstable direction. For flows with slowly evolving coherent features which exhibit a disparity between fast Lagrangian and slow Eulerian timescales, the results of Figs. 1d and 2 show that either the finite-scale Lyapunov exponent or the location of frozen time Eulerian saddle points may be used as surrogates for computing numerical manifolds.

4. Numerical experiments

The dependence of assimilation performance on drifter launch location is assessed in a series of twin experiment simulations. In each, the basic model is integrated past initial transients to some initial condition time-stamped $t = 0$ and then forward for 30 days. This Control run provides both

a means for producing synthetic drifter data and for benchmarking Eulerian fields against which to measure the assimilation experiments.

The assimilation, Assim, and Control simulations are identical model, different initial condition comparisons. In experiment IC1, the assimilation starts from rest; zero velocity and constant layer depth fields at $t = 0$. In experiment IC2, the initial conditions for the assimilation are provided by Control model output at a time in the second year of simulation ($t = 730$ days). In each case, various sets of synthetic drifter data provided by the Control velocity field are input to the assimilation (Assim). In order to separate basic model performance from assimilation efficiency, the model is also integrated forward from each of the assimilation initial conditions without data input (Noassim).

For each of the assimilation initial conditions, experiments are conducted for 51 different sets of Lagrangian data. The choice of the geometry of the initial drifter launch locations and the total amount of drifter data provided to the assimilation is driven by the knowledge of the Lagrangian structures provided in Section 3 and the desire to mimic expected operational scenarios involving a relatively limited number of drifters. The directed launch strategy locates three sets of four drifters initialized on lines of length $l = 20$ km centered at the three hyperbolic trajectories shown in Fig. 2. For comparison, in each of the other 50 launch experiments, four drifters are initialized on randomly oriented lines of length l centered at three randomly chosen points in the energetic, eddy shedding region near the separating boundary current.

In all cases, the data sampling period of the assimilation is fixed at $\Delta t = 6$ h less than the Lagrangian time-scale of the flow. The efficiency of the assimilation measured by the ratio of the area averaged velocity differences:

$$\epsilon_{\mathrm{rel}}(t) = \frac{\mathrm{ER}_{\mathrm{control-assim}}(t)}{\mathrm{ER}_{\mathrm{control-noassim}}(t)}, \tag{3}$$

where $\mathrm{ER}_{\mathrm{control-assim}}(\mathrm{ER}_{\mathrm{control-noassim}})$ represents the rms of the velocity difference between control and assim (noassim) defined as:

$$\mathrm{ER}_{\mathrm{control-assim}}(t) = \sqrt{K^{-1}\sum_{i}^{K}\left[(u_i^{\mathrm{control}}(t) - u_i^{\mathrm{assim}}(t))^2 + (v_i^{\mathrm{control}}(t) - v_i^{\mathrm{assim}}(t))^2\right]}, \tag{4}$$

where u_i, v_i are the model velocity components at gridpoint i and K is the total number of gridpoints.

It is found that there is no significant difference between the error measured with the layer thickness or the velocity variables. Hence only the velocity error is employed in the assimilation performance analysis.

5. Results

5.1. Performance of the directed launch strategy

The results for both assimilation initial conditions (IC1 and IC2) are shown in Fig. 3 for three different sets of Lagrangian data. The first row shows the evolution of the layer depth

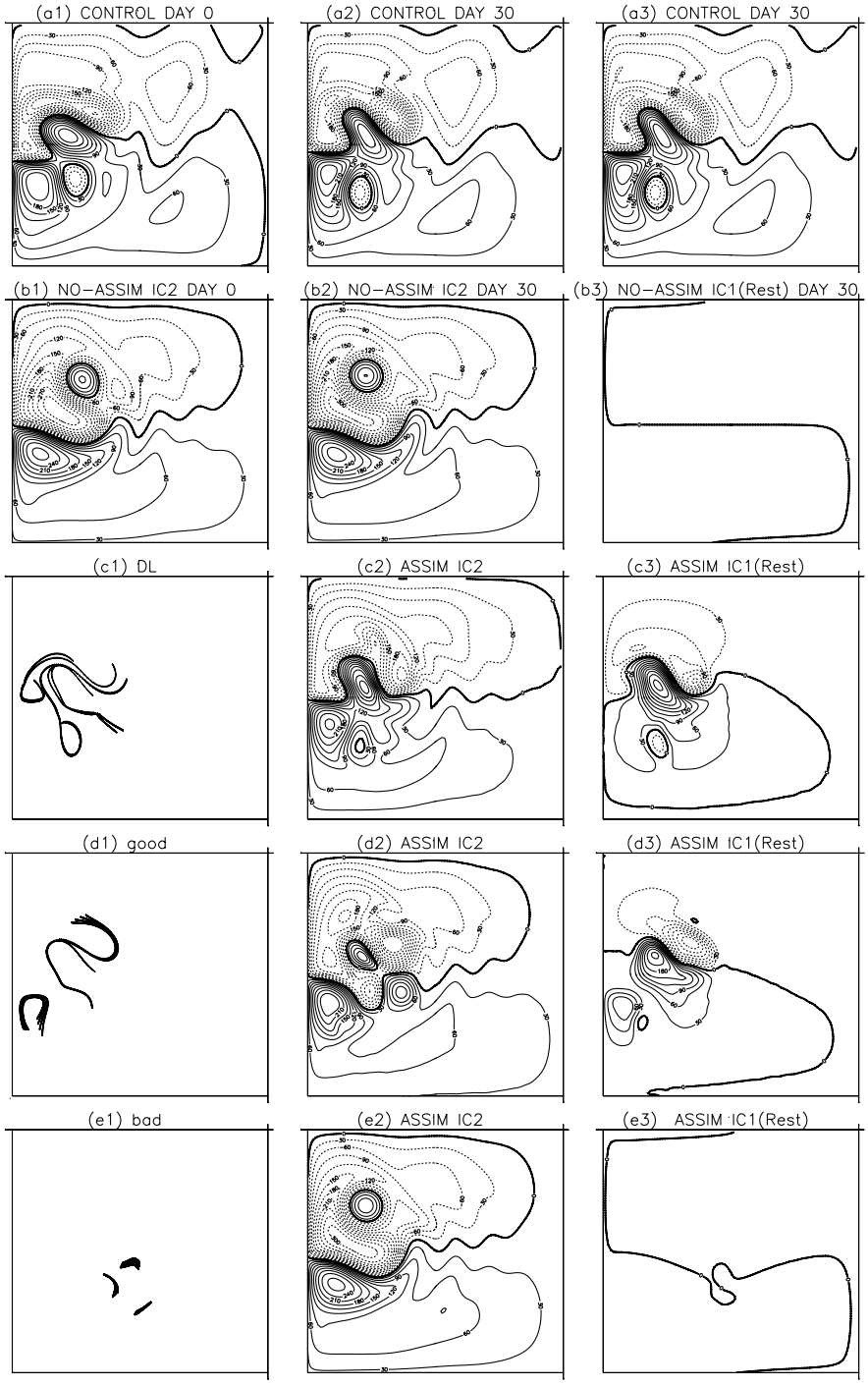

Fig. 3. (a1, a2, a3) Time evolution of Control, (b1, b2, b3) time evolution of Noassim for both IC2 and IC1. 30-day Lagrangian trajectories and snapshots of the layer thickness in Assim for both IC1 and IC2 cases for (c1, c2, c3) directed launch case, (dl, d2, d3) a 'good' case, and (e1, e2, e3) a 'bad' case selected from random launches.

field in the control run over the 30 days of interest with the final state repeated for ease of comparison. The second row shows the layer depth field for the initial condition IC2 and its evolution *without* assimilation as well as the 30 day evolution of IC1 (rest) without assimilation.

Rows (c), (d) and (f) of the figure indicate the 30-day trajectories of three different drifter launch experiments in the first column, as well as the corresponding assimilation results for IC1 and IC2 on the final day. Comparison between the resulting layer depth fields and those of the control run in the first row provides a visual measure of assimilation efficiency.

Row (c) of the figure shows the trajectories and resulting assimilation layer depth fields for the *Directed Launch* (DL) strategy where the initial drifter locations were chosen along the unstable directions of the three hyperbolic trajectories found in Section 3. As seen in figure (c1), this directed launch leads to high data coverage in the domain and Lagrangian information about the boundaries of the coherent features in the flow field. This Lagrangian structure information leads to qualitative improvements in both assimilation experiments.

For IC2, where the assimilation starts from the 'wrong' initial conditions, comparison of figure (c2) to the control field in (a2) indicates that the Lagrangian data has, in 30 days, lead to an accurate prediction of jet meander size and shape, the elimination of the strong fictitious warm core eddy in the sub-polar gyre (b2) and the development of a cold core ring at the correct location in the sub tropical gyre. For IC1, where the assimilation spins up from rest, comparison of figure (c3) with (a3) again indicates that the Lagrangian data supplied by the directed launch strategy provides essential structure information. After 30 days, the assimilation gives a qualitatively correct shape for the meandering central jet and indications of the presence of a cyclonic eddy in the sub-tropical gyre.

For comparison, the results for two other sets of drifter initial conditions are shown in rows (d) and (e), chosen for their respectively low (high) values of the globally integrated assimilation error ϵ_{rel} at time $t = 30$ days. Again, comparison of the assimilation layer depth fields to the control provides a qualitative means of judging assimilation performance. Notably, the set of trajectories of the 'good' launch locations shown in row (d) share some properties of the directed launches, spending time within the energetic jet region and sampling, in part, the hyperbolic region around the cyclone in the subpolar gyre. The 'bad' launch set, not surprisingly, fails to sample any of the energetic structures in the flow.

The time trace of the integrated error ratio for the three sets of drifter data is shown in Fig. 4. In the spin up experiment (Fig. 4a), assimilating data from the directed launches is suboptimal in comparison to several of the randomly launched sets during the first 5–10 days of the assimilation runs. Seeding drifters in the vicinity of hyperbolic trajectories implies low initial kinetic energy for the drifters and thus limits the data driven forcing. As the directed drifter trajectories evolve and distribute themselves along the unstable manifolds, they eventually sample high kinetic energy regions of the flow providing the input data that is optimal in terms of the basin averaged energy error over the 51 experiments conducted.

As shown in Fig. 4b, the effect of initially low drifter kinetic energy is less pronounced in IC2 experiments where assimilating the distribution of low velocity values is essential to correct the imposed initial flow state. While the directed launch data is again suboptimal for short times, directly sampling the boundaries of the coherent features eventually leads to a marked improvement in the assimilation error for later times.

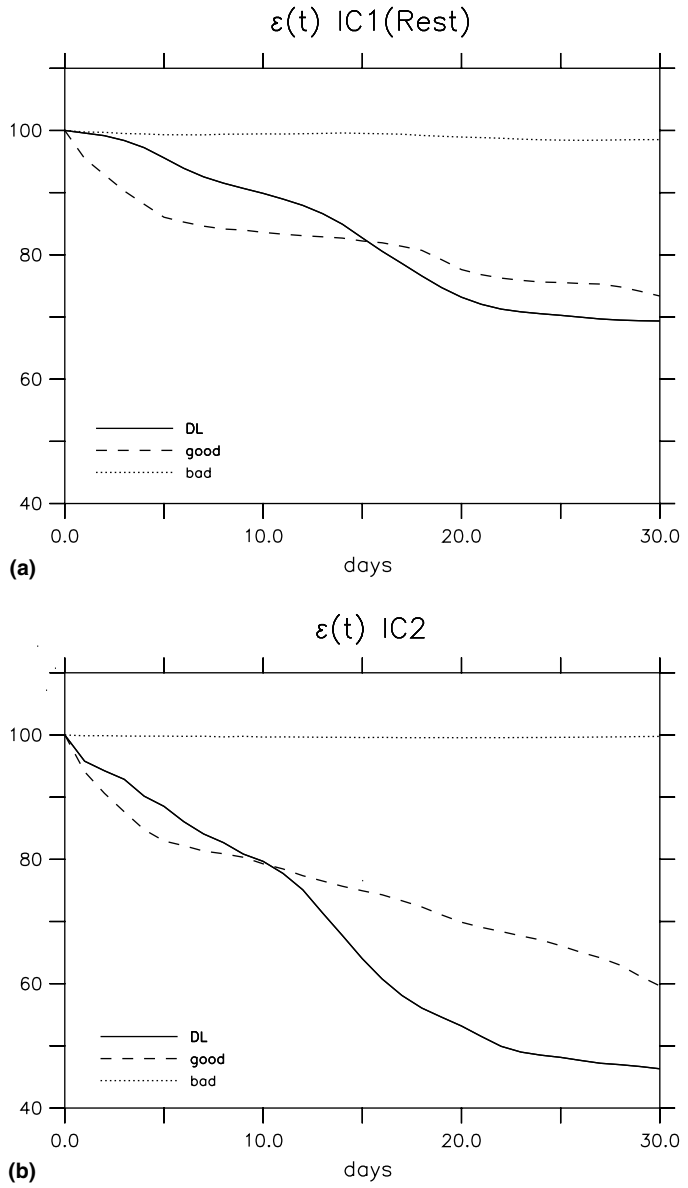

Fig. 4. Time traces of error $\epsilon_{rel}(t)$ (in %) for the 'bad' case (dotted lines), 'good' case (dashed lines) and directed launch case (solid lines) for IC1 (a) and IC2 (b) twin experiments.

5.2. Lagrangian performance diagnostics

In an effort to determine what integral properties of the drifter data contribute to efficient assimilation, several drifter diagnostics are computed: overall data coverage, N, drifter kinetic energy, KE, the difference between the observed and simulated drifter positions, dr, and the product

dr$N$. This last quantity serves as a proxy for the actual data correction term used in the assimilation procedure.

The overall data coverage is defined by first binning the energetic western boundary separation region into $n = 15 \times 16$ square boxes of 4×4 grid points (80×80 km). Data coverage, N, is computed by counting the total number of bins that contain at least one drifter at any time during the interval of interest.

$$N = \int \sum_{i=1}^{n} I(i,t)\mathrm{d}t, \tag{5}$$

where $I(i,t)$ is an indicator function in each bin equal to 1 if the bin contains at least one drifter at time t and equal to zero otherwise. In other words, N is the number of bins visited by drifters following the initial launch throughout the observation period, and it provides a measure of the overall spread of the drifters and means of quantifying the spatial independence of the Lagrangian data.

The integrated kinetic energy is computed by interpolating the Eulerian velocity at the drifter position. With n_d given by the number of drifters in each experiment,

$$\mathrm{KE} = \int \frac{1}{n_\mathrm{d}} \left(\sum_{i=1}^{n_\mathrm{d}} u_i(t)^2 + v_i(t)^2 \right) \mathrm{d}t. \tag{6}$$

A measure of the *persistence* of the Lagrangian data in the assimilation is given by the integrated distance between the drifter observations, x^o and the simulated model trajectories, x defined as:

$$\mathrm{dr} = \int \sum_{i=1,n_\mathrm{d}} \sqrt{(x(i,t) - x^\mathrm{o}(i,t))^2 + (y(i,t) - y^\mathrm{o}(i,t))^2}\,\mathrm{d}t. \tag{7}$$

This quantity determines the time integrated size of the data-driven correction term in the assimilation. Drifter data sets which continually seed uncorrected portions of the flow field are expected to provide larger corrections and more accurate assimilations.

The product of the overall coverage N and the integrated distance difference dr,

$$\mathrm{Corr} = \mathrm{dr}N \tag{8}$$

provides a proxy for both terms in the overall assimilation correction given by Eq. (7) with dr approximating the Lagrangian velocity difference and N corresponding to the γ spreading term.

Scatter plots of the 30-day error ratio $\epsilon_\mathrm{rel}(t = 30 \text{ days})$ versus each of the diagnostics are shown in Fig. 5 for all 51 different initial launch experiments. The first column indicates results for assimilations starting from rest (IC1), while the second column shows results for the energetic initial condition (IC2). In each scatter plot, the directed launch strategy is represented by the symbol (*) which is also characterized by the lowest error. Also shown is the best fit least squares line and correlation coefficient.

As expected, assimilation errors correlate well with each of the diagnostics and the highest correlator for both initial conditions is the integrated distance difference, dr. Notably, the strong correlation of error with both coverage and kinetic energy for the spin-up experiment is reduced when the initial assimilation field already contains velocity information (IC2).

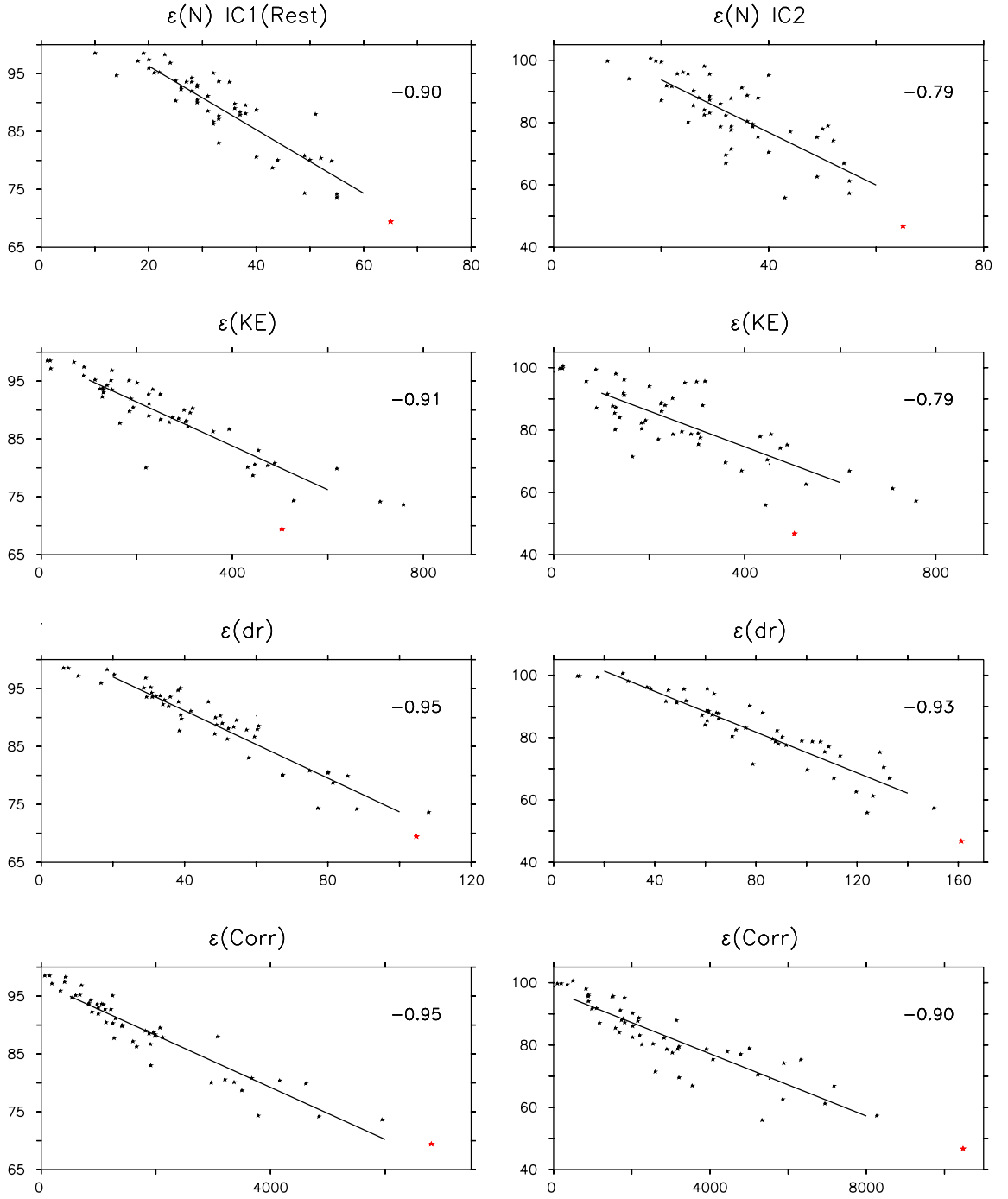

Fig. 5. Scatter plots of $\epsilon_{rel}(t = 30$ days) (in %) versus N (top, first row), versus KE (second row), versus dr (third row), versus Corr (fourth row), for IC1 (left column) and IC2 (right column) twin experiments. Red (⋆) symbols denote the values from directed launch experiments. Correlation coefficients are shown in the upper right corner of each figure. (For interpretation of the references in colour in this figure legend, the reader is referred to the web version of this article.)

For both assimilation initial conditions, the data produced by the directed launch strategy provides the minimum error ratio at 30 days over all 51 launch experiments. For the spin-up case, IC1, the directed launch provides approximately a 22% decrease in error from the mean of the 50 random launch experiments. In the case of IC2, where assimilation of the coherent structure boundaries is more critical, the directed launch lead to an approximately 40% decrease in the error when compared to the mean error ration of the random launches. Given the qualitative comparisons of layer depth fields shown in Fig. 3, one might expect even larger improvements if a more structure sensitive error measure were employed.

As shown, directing drifter initial conditions along unstable directions in hyperbolic regions produces drifter data with maximum data sampling and maximum persistence as measured by dr. Although such launches, by design, start in low kinetic energy regions, they rapidly disperse along directions that foliate boundaries of energetic structures.

5.3. Sensitivity experiments

As seen in Figs. 1 and 2, there exists small but measurable differences between the positions of frozen time Eulerian saddle points, intersections of maximal forward and backward time FSLE regions, and the intersections of the numerically generated stable and unstable manifolds. In fact, for finite-time data sets, the manifolds themselves are non-unique to exponential order in the existence time and Eulerian hyperbolicity. In light of the uncertainties inherent in locating the

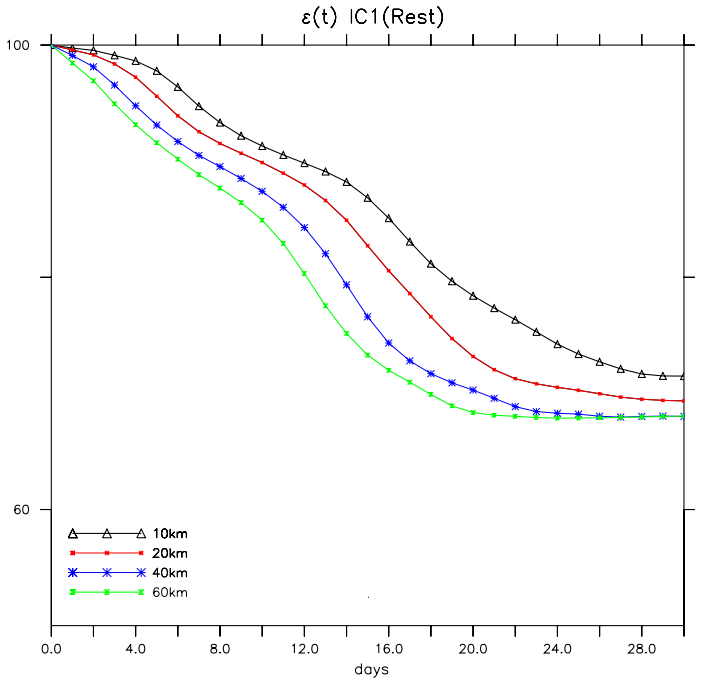

Fig. 6. Dependence of assimilation error $\epsilon_{rel}(t)$ (in %) on the length of initial launch segments ($l = 10$ km: black line, $l = 20$ km: red line, $l = 30$ km: blue line, $l = 40$ km: green line).

hyperbolic trajectories and to investigate the feasibility of using surrogates such as FSLE fields, we test the sensitivity of the assimilation results to the length of the initial line segments and the vicinity (in both distance and orientation) of the seeding to the location of the hyperbolic trajectory and unstable direction.

Fig. 6 shows the evolution of ϵ_{rel} for the directed launch experiment conducted with increasing initial segment lengths for assimilations started from rest. The shapes are similar in all cases, since the segments are straddling the hyperbolic points. Fig. 6 shows that the short-term performance of the assimilation scheme improves somewhat when longer seeding segments are used, since the initial coverage becomes greater and the time necessary for the initial dispersion of the drifters is reduced when the segment length is increased.

The directed launch results are based on determining the intersection and orientation of Lagrangian manifolds computed directly from the control flow. In practice, such information would only result from predictive estimates of an assimilating model and additional input data (sea-surface height, for example), which are both subject to error. To determine the sensitivity of the directed launch results to errors in initial placement and orientation, we consider the spin-up experiment, IC1 case, with an initial segment length of $l = 20$ km. The location of the mid point of each of the three launch segments is varied a distance from 10 to 100 km

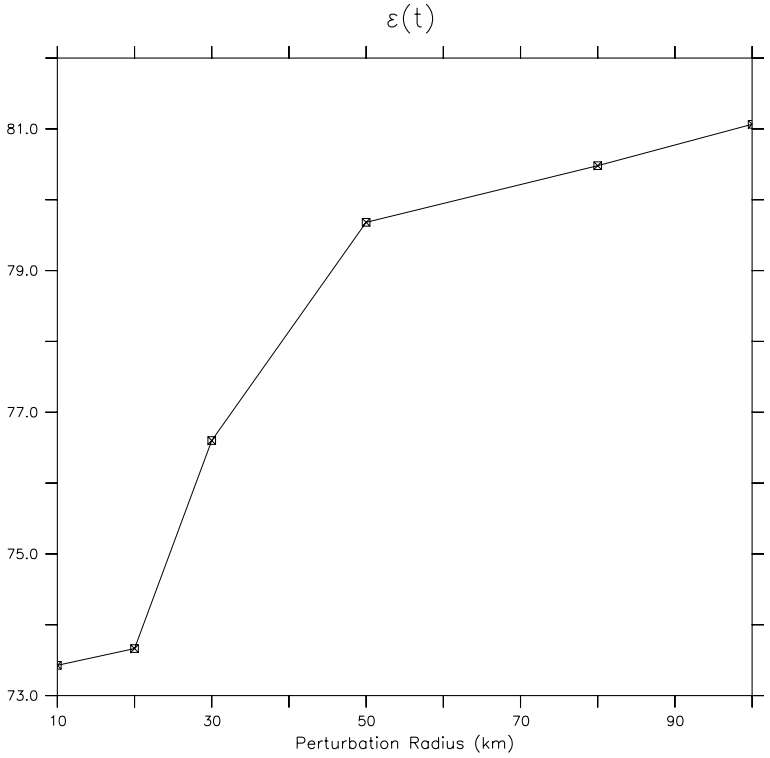

Fig. 7. $\epsilon_{rel}(t = 30$ days) (in %) as a function of the perturbation distance of the initial launch location from the "ideal" directed launch along the exact unstable manifolds.

around the hyperbolic trajectory, with an orientation randomly chosen within $\pi/4$ radians from the correct one. Results of this sensitivity experiments are shown in Fig. 7. Not surprisingly, if the error in location is less than the 20 km segment length, the efficiency of the launching is assured. With increasing location error, the performance of the strategy is decreased, but still an improvement over random launch experiments is evident. If the hyperbolic points are predicted by the OGCM with an error of 100 km, the error in the directed launches (approximately 81%) remains well below the median value of that produced by the 50 random launch experiments.

6. Summary and conclusions

A number of new assimilation techniques have been recently proposed to take advantage of the increasing amount of Lagrangian position data available in the world's ocean. Studies by Molcard et al. (2003, 2005) have been conducted by launching synthetic drifters simultaneously in regularly-spaced arrays in high kinetic energy regions of the flow field. The main objective for such launch configuration was to minimize the sensitivity of the results to drifter launch locations, and to focus on the technical aspects of data assimilation method development. Nevertheless, not only are the results sensitive to the locations of drifter deployment (unless a very high number of drifters are used), but also simultaneous deployment of drifters at dozens of locations, that are O(100 km) apart from one another, is not feasible in practice.

In light of these considerations, the primary objective of the present study is to address the basic and practical question of determining the initial drifter lunch locations that would increase the performance of the Lagrangian assimilation scheme in data-limited applications. In contrast to the previous works of Poje et al. (2002) and Toner and Poje (2004) on structure based launch schemes which used proxies such as Eulerian field reconstruction and sampled velocity distribution functions as proxies for assimilation performance, the present study examines the advantages of optimized launch schemes directly in terms of assimilation output. The study is conducted in two stages: the first stage is devoted to the identification of hyperbolic trajectories and high dispersion regions in the flow field, and the second stage is devoted to an experimental procedure to determine whether launch strategies targeted at hyperbolic regions provides significant advantages for Lagrangian data assimilation.

The strongest hyperbolic regions in the energetically active part of the flow field are identified by directly calculating numerical analogs of the finite-time stable and unstable manifolds emanating from hyperbolic trajectories. It is shown that the Lagrangian hyperbolic trajectory is well approximated by the location of saddle-type equilibrium points that can be identified from the Eulerian flow field, since the Lagrangian time scales are much faster than the Eulerian time scales, FSLE, an alternative means of identifying high dispersion regions in the flow field (Aurell et al., 1997; Artale et al., 1997) are also calculated, and it is shown that there is a strong correlation between the geometry of the in-flowing (out-flowing) manifolds and minimum (maximum) values of the FSLE.

Given this knowledge of the location of the Lagrangian structures, line segments along the unstable directions of the hyperbolic trajectories are seeded with drifters. The strongest three

hyperbolic trajectories are used, the length of the line segments are taken as 20 km, and each segment is seeded with four equally-spaced drifters (a total of 12 drifters are assimilated). The results from this directed launch strategy are compared to those from 50 other randomly-oriented sets of line segments (three segments with four drifters each) in the energetic region of the flow field. The performance of the assimilation scheme is quantified using the so-called twin experiment approach, in which drifters sampling the Control experiment are assimilated into the Assim experiment, started with identical model parameters but from different initial conditions. The efficiency of the assimilation is quantified by the ratio of the rms difference between the velocity fields of Control and Assim, and that of Control and Noassim (the experiment which depicts the evolution of the flow field in the absence of drifter assimilation).

It is found that the convergence of the Lagrangian assimilation scheme is consistently and significantly improved by such directed launches compared to randomly selected initial drifter positions. By directing initial drifter positions along the out-flowing branch of identifiable Lagrangian boundaries, the relative dispersion of the drifters, the overall data-coverage and the sampling of high kinetic energy features in the flow are optimized. In general, the performance of the assimilation procedure is shown to depend strongly on the independence of the observed drifter trajectories and the temporal persistence of the corrections provided by the data.

Given the potential uncertainties in identifying hyperbolic trajectories in practical oceanic situations, the sensitivity of the results to the length of seeding segments, and vicinity (both in terms of distance and orientation) with respect to the unstable directions of the hyperbolic trajectories is investigated. It is found that the short-term performance of the assimilation scheme improves somewhat when longer seeding segments are used, since the initial coverage becomes greater and the time necessary for the initial dispersion of the drifters is reduced when the segment length is increased. Finally, it is found that there is no significant change in the assimilation performance when position errors up to half of the radius of deformation are introduced in the initial location of the segments, with respect to the unstable manifolds of the hyperbolic trajectories.

In conclusion, we have shown that when Lagrangian coherent features in the flow field introduce high dispersion areas, the identification of these areas via Eulerian saddle points, FSLE or Lagrangian hyperbolic trajectories, leads to a systematic procedure to improve the information content of limited amounts of Lagrangian data for assimilation in OGCMs.

Combination of these Lagrangian techniques with recent advances in Lagrangian data assimilation to improve the forecasting accuracy of OGCMs is potentially fruitful for many practical applications, and our future goals include incorporation of these methods in realistic OGCMs for use in observational field programs.

Acknowledgements

A. Molcard and T. Özgökmen greatly appreciate the support of ONR via grants N00014-99-1-0049 and N00014-03-1-0285. A. Molcard was also supported by the EC project "stirring and mixing in turbulence". A.C. Poje was supported by NSF grant ATM-200102 and ONR grant N00014-00-0019.

Appendix A

In the reduced-gravity configuration, MICOM integrates the following momentum and layer-thickness conservation equations:

$$\frac{\partial u}{\partial t} + \mathbf{u}\cdot\nabla u - fv = -g'\frac{\partial h}{\partial x} + \rho^{-1}\frac{\partial \tau^x}{\partial z} + \nu_{\mathrm{H}} h^{-1}\nabla\cdot h\nabla u, \tag{9}$$

$$\frac{\partial v}{\partial t} + \mathbf{u}\cdot\nabla v + fu = -g'\frac{\partial h}{\partial y} + \rho^{-1}\frac{\partial \tau^y}{\partial z} + \nu_{\mathrm{H}} h^{-1}\nabla\cdot h\nabla v, \tag{10}$$

$$\frac{\partial h}{\partial t} + \nabla\cdot(\mathbf{u}h) = 0, \tag{11}$$

where $\mathbf{u} = (u, v)$ is the layer-averaged horizontal velocity vector, h the thickness of a layer of constant density, $g' = g\frac{\Delta\rho}{\rho}$ the reduced gravity, g gravitational acceleration, ρ the layer density, $\Delta\rho$ the density difference between the active and motionless layers, $f = f_0 + \beta_0 y$ the Coriolis frequency with beta-plane approximation, $\boldsymbol{\tau} = (\tau^x, \tau^y)$ the wind stress vector, and ν_{H} the lateral viscosity coefficient.

The optimal interpolation method used as the basis for the Lagrangian data assimilation technique is based on the general Bayesian theory (e.g., Lorenc, 2000):

$$\mathbf{u}^{\mathrm{a}} = \mathbf{u}^{\mathrm{b}} + \mathbf{R}^{\mathrm{b}}\mathbf{G}^{\mathrm{T}}(\mathbf{G}\mathbf{R}^{\mathrm{b}}\mathbf{G}^{\mathrm{T}} + \mathbf{R}^{\mathrm{o}})^{-1}(\mathbf{y} - \mathbf{H}(\mathbf{u}^{\mathrm{b}})), \tag{12}$$

where $\mathbf{u}^{\mathrm{a}}$ is the Eulerian model velocity vector after assimilation, $\mathbf{u}^{\mathrm{b}}$ is the model velocity vector before assimilation, $\mathbf{y}$ is the vector of observations, $\mathbf{H}(\mathbf{u}^{\mathrm{b}})$ is the model counterpart, e.g., the measurement functional/model, $\mathbf{R}^{\mathrm{o}}$ is the observation error covariance matrix, $\mathbf{R}^{\mathrm{b}}$ is the covariance matrix of the model uncertainty, superscript T stands for transposition, and, finally $\mathbf{G} = \frac{\delta\mathbf{H}(\mathbf{u}^{\mathrm{b}})}{\delta\mathbf{u}^{\mathrm{b}}}$ is the derivative of the model-to-observation functional (sensitivity matrix). Consider M Lagrangian particles released at the same time $t = 0$ from different positions $\mathbf{r}_1^0, \mathbf{r}_2^0, \ldots, \mathbf{r}_M^0$ in an isopycnic layer l. The M particles provide information on their position $\mathbf{r}_m^t (m = 1, M)$ at discrete times t with sampling interval Δt. The average Lagrangian velocity during Δt can then be computed by finite difference of two successive positions, $\mathbf{v}_m(t) = (\mathbf{r}_m^{t+1} - \mathbf{r}_m^t)/\Delta t (m = 1, M)$.

Under simplifying assumptions given in detail in Molcard et al. (2003), Eq. (12) can be simplified to

$$\mathbf{u}^{\mathrm{a}} = \mathbf{u}^{\mathrm{b}} + \Delta\mathbf{u} \tag{13}$$

with

$$\Delta\mathbf{u}(i, j, n) = \frac{\sigma_{\mathrm{b}}^2}{\sigma_{\mathrm{b}}^2 + \sigma_{\mathrm{o}}^2}\sum_{m=1}^{M}\gamma_{ijm}(\mathbf{v}_m^{\mathrm{o}}(n) - \mathbf{v}_m^{\mathrm{b}}(n)), \tag{14}$$

where

$$\gamma_{ijm} = E_h(x_m^{\mathrm{b}}(n) - ih, y_m^{\mathrm{b}}(n) - jh), \quad E_h(x, y) \equiv \exp\left(-\frac{x^2}{2r^2} - \frac{y^2}{2r^2}\right), \tag{15}$$

where the indexes i, j indicate the Eulerian grid point, n the discrete time $n\Delta t$, $n = 1$, N, and l is the layer in which the Lagrangian particles are released. $\mathbf{v}^{\mathrm{o}}$ and $\mathbf{v}^{\mathrm{b}}$ are the observations (o) and model

(b) Lagrangian velocity respectively, and $\mathbf{v}^{\mathrm{b}}$ is computed in the model by generating trajectories during Δt and using the two end points, σ_{b}^2 is the model velocity mean square error and σ_{o}^2 is the error for the Lagrangian velocity that is related to the error of independent positions, say, σ_r^2, by $\sigma_{\mathrm{o}}^2 = \frac{\sigma_r^2}{\Delta t}$. The observation and model error ratio is taken as $\frac{\sigma_r^2}{\sigma_{\mathrm{b}}^2} = 10^5\ \mathrm{s}^2$. Since there are no accurate estimates of such error from Lagrangian observation systems, this parameter is estimated from empirical values for observation and model errors, and introducing such error in the assimilation scheme will not affect the relative performance of different launches.

The assimilation formula for the layer thickness is

$$h^{\mathrm{a}}(n) = h^{\mathrm{b}}(n) + \Delta h_g - \Delta m, \tag{16}$$

where

$$\nabla^2(\Delta h_g) = \frac{f}{g'}\left[\frac{\partial(\Delta v)}{\partial x} - \frac{\partial(\Delta u)}{\partial y}\right] \tag{17}$$

is solved subject to homogeneous boundary conditions, and

$$\Delta m = \frac{1}{|A|}\int_A \Delta h_g \,\mathrm{d}A, \tag{18}$$

where A is the considered ocean basin and $|A|$ its area.

References

Aref, H., 1984. Stirring by chaotic advection. J. Fluid Mech. 192, 115–173.

Artale, V., Boffetta, G., Celani, A., Cencini, M., Vulpiani, A., 1997. Dispersion of passive tracers in closed basins: beyond the diffusion coefficient. Phys. Fluids 9, 3162–3171.

Aurell, E., Boffetta, G., Crisanti, A., Paladin, G., Vulpiani, A., 1997. Predictability in the large: an extension of the concept of Lyapunov exponent. J. Phys. A 30, 1–26.

Bauer, S., Swenson, M., Griffa, A., 2003. Eddy mean flow decomposition and eddy diffusivity estimates in the Tropical Pacific Ocean: 2 results. J. Geophys. Res. 107, 3154.

Bleck, R., Chassignet, E.P., 1994. Simulating the oceanic circulation with isopycnic-coordinate models. In: Majumdar, S.K., Miller, E.W., Forbes, G.S., Schmalz, R.F., Panah, A.A. (Eds.), The Oceans: Physical–Chemical Dynamics and Human Impact. The Pennsylvania Academy of Science, pp. 17–39.

Bleck, R., Rooth, C., Hu, D., Smith, L.T., 1992. Salinity-driven transients in a wind- and thermohaline-forced isopycnic coordinate model of the North Atlantic. J. Phys. Oceanogr. 22, 1486–1505.

Coulliette, C., Wiggins, S., 2000. Intergyre transport in a wind-driven, quasigeostrophic double gyre: an application of lobe dynamics. Nonlinear Process. Geophys. 7, 59–85.

Davis, R., 1985. Drifter observations of coastal currents during CODE: the statistical and dynamical views. J. Geophys. Res. 90, 4756–4772.

Davis, R., 1991. Observing the general-circulation with floats. Deep Sea Res. 38, 531–571.

Davis, R.E., 1996. Comparison of Autonomous Lagrangian Circulation Explorer and fine resolution Antarctic model results in the South Atlantic. J. Geophys. Res. Oceans 101 (C1), 855–884.

Davis, R., 1998. Preliminary results from directly measuring mid-depth circulation in the Tropical and South Pacific. J. Geophys. Res. Oceans 103, 24619–24639.

Fratantoni, D., 2001. North Atlantic surface circulation during the 1990s observed with satellite-tracked drifters. J. Geophys. Res. 106, 22067–22093.

Garraffo, Z., Mariano, A., Griffa, V.C., Chassignet, E., 2001. Lagrangian data in a high-resolution numerical simulation of the North Atlantic I. Comparison with in situ drifter data. J. Marine Syst. 29, 157–176.

Griffa, A., 1996. Applications of stochastic particle models to oceanographic problems. In: Adler, R., Muller, P., Rozovskii, B. (Eds.), Stochastic Modelling in Physical Oceanography. Birkhauser.

Haller, G., Poje, A., 1998. Finite time transport in aperiodic flows. Physica D 119, 352–380.

Hansen, D., Maul, G., 1991. Anticyclonic current rings in the eastern tropical Pacific Ocean. J. Geophys. Res. 9, 6965–6979.

Hernandez, F., Le Traon, P.-Y., Barth, N., 1995. Optimizing a drifter cast strategy with a genetic algorithm. J. Atmos. Ocean. Technol. 12, 330–345.

Ide, K., Ghil, M., 1997a. Extended Kalman filtering for vortex systems. Part I: Methodology and point vortices. Dyn. Atmos. Oceans 27, 301–332.

Ide, K., Ghil, M., 1997b. Extended Kalman filtering for vortex systems. Part II: Rankine vortices and observing system design. Dyn. Atmos. Oceans 27, 333–350.

Ide, K., Kuznetsov, L., Jones, C., 2002. Lagrangian data assimilation for point vortex systems. J. Turbul. 3, 53.

Ishikawa, Y.I., Awaji, T., Akimoto, K., 1996. Successive correction of the mean sea surface height by the simultaneous assimilation of drifting buoy and altimetric data. J. Phys. Oceanogr. 26, 2381–2397.

Kamachi, M., O'Brien, J., 1995. Continuous assimilation of drifting buoy trajectory into an equatorial pacific ocean model. J. Mar. Syst. 6, 159–178.

Kuznetsov, L., Ide, K., Jones, C., 2003. A method for the assimilation of Lagrangian data. Mon. Weather Rev. 131, 2247–2260.

Lavender, K., Davis, R., Owens, W., 2002. Observations of deep convection in the Labrador Sea from subsurface floats. J. Phys. Oceanogr. 32, 511–526.

Lorenc, A.C., 2000. A Bayesian approach to observation quality control in variational and statistical assimilation. Paper presented at Aha Huliko Hawaiian Winter Workshop, Univ. of Hawaii, Honolulu, Hawaii.

McClean, J., Poulain, P.-M., Pelton, J., 2002. Eulerian and Lagrangian statistics from surface drifters and a high-resolution POP simulation in the North Atlantic. J. Phys. Oceanogr. 32, 2472–2491.

Miller, P., Jones, C., Rogerson, A., Pratt, L., 1997. Quantifying transport in numerically generated velocity fields. Physica D 110, 105–122.

Miller, P., Pratt, L., Helfrich, K., Jones, C., 2002. Chaotic transport of mass and potential vorticity for an island recirculation. J. Phys. Oceanogr. 32, 80–102.

Molcard, A., Piterbarg, L., Griffa, A., Özgökmen, T.M., Mariano, A.J., 2003. Assimilation of drifter positions for the reconstruction of the Eulerian circulation field. J. Geophys. Res. 108 (3), 3056.

Molcard, A., Griffa, A., Özgökmen, T.M., 2005. Lagrangian data assimilation in multilayer primitive equation ocean models. J. Ocean Atmos. Technol. 22 (1), 2006–2026.

Niiler, P.P., Maximenko, N.A., Panteleev, G.G., Yamagata, T., Olson, D.B., 2003. Near surface dynamical structure of the Kuroshio extension. J. Geophys. Res. Oceans 108 (C6). Art. No. 3193.

Oschlies, A., Willebrand, J., 1996. Assimilation of Geostat altimeter data into an eddy-resolving primitive equation model of the North Atlantic Ocean. J. Geophys. Res. 101, 14175–14190.

Owens, W., 1991. A statistical description of the mean circulation and eddy variability in the northwestern Atlantic using SOFAR floats. Prog. Oceanogr. 28, 257–303.

Özgökmen, T., Molcard, A., Chin, T., Piterbarg, L., Griffa, A., 2003. Assimilation of drifter observations in primitive equation models of mid-latitude ocean circulation. J. Geophys. Res. 108, 3238.

Poje, A., Haller, G., 1999. Geometry of cross-stream mixing in a double-gyre ocean model. J. Phys. Oceanogr. 29, 1649–1665.

Poje, A.C., Toner, M., Kirwan, A.D., Jones, C.K.R.T., 2002. Drifter launch strategies based on Lagrangian templates. J. Phys. Oceanogr. 32, 1855–1869.

Poulain, P., 1993. Estimates of horizontal divergence and vertical velocity in the equatorial Pacific. J. Phys. Oceanogr. 23, 601–607.

Poulain, P., Luther, D., Patzert, W., 1992. Deriving inertial wave characteristics from surface drifter velocities–frequency variability in the Tropical Pacific. J. Geophys. Res. 97, 17947–17959.

Reverdin, G., Niiler, P., Valdiimasson, H., 2003. North Atlantic Ocean surface currents. J. Geophys. Res. 108, 3002.

Richardson, P.L., 1993. A census of eddies observed in North Atlantic SOFAR float data. Prog. Oceanogr. 31, 1–50.

Richardson, P., 2001. Drifters and floats. Encycloped. Ocean Stud. 2, 767–774.
Samelson, R., 1991. Fluid exchange across a meandering jet. J. Phys. Oceanogr. 21, 431–440.
Smith, R., Maltrud, M., Bryan, F., Hecht, M., 2000. Numerical simulation of the North Atlantic ocean at 1/10°. J. Phys. Oceanogr. 30, 1532–1561.
Toner, M., Poje, A.C., 2004. Lagrangian velocity statistics of directed launch strategies in a Gulf of Mexico model. Nonlinear Process. Geophys. 11, 35–46.
Veneziani, C., Griffa, A., Reynolds, A., Mariano, A., 2004. Oceanic turbulence and stochastic models from subsurface Lagrangian data the North-West Atlantic Ocean. J. Phys. Oceanogr. 34.
Zhang, H., Prater, M., Rossby, T., 2001. Isopycnal Lagrangian statistics from the North Atlantic Current RAFOS float observations. J. Geophys. Res. 106, 13817–13836.
Zhou, M., Niiler, P., Hu, J., 2002. Surface currents in the Bransfield and Gerlaeche Straits, Atlantica. Deep Sea Res. 49, 267–280.